LETTER

doi:10.1038/nature14242

Fundamental properties of unperturbed haematopoiesis from stem cells *in vivo*

Katrin Busch[1], Kay Klapproth[1]*, Melania Barile[2]*, Michael Flossdorf[2]*, Tim Holland-Letz[3], Susan M. Schlenner[4,5], Michael Reth[6,7], Thomas Höfer[2] & Hans-Reimer Rodewald[1]

Haematopoietic stem cells (HSCs) are widely studied by HSC transplantation into immune- and blood-cell-depleted recipients. Single HSCs can rebuild the system after transplantation[1–5]. Chromosomal marking[6], viral integration[7–9] and barcoding[10–12] of transplanted HSCs suggest that very low numbers of HSCs perpetuate a continuous stream of differentiating cells. However, the numbers of productive HSCs during normal haematopoiesis, and the flux of differentiating progeny remain unknown. Here we devise a mouse model allowing inducible genetic labelling of the most primitive Tie2$^+$ HSCs in bone marrow, and quantify label progression along haematopoietic development by limiting dilution analysis and data-driven modelling. During maintenance of the haematopoietic system, at least 30% or ~5,000 HSCs are productive in the adult mouse after label induction. However, the time to approach equilibrium between labelled HSCs and their progeny is surprisingly long, a time scale that would exceed the mouse's life. Indeed, we find that adult haematopoiesis is largely sustained by previously designated 'short-term' stem cells downstream of HSCs that nearly fully self-renew, and receive rare but polyclonal HSC input. By contrast, in fetal and early postnatal life, HSCs are rapidly used to establish the immune and blood system. In the adult mouse, 5-fluoruracil-induced leukopenia enhances the output of HSCs and of downstream compartments, thus accelerating haematopoietic flux. Label tracing also identifies a strong lineage bias in adult mice, with several-hundred-fold larger myeloid than lymphoid output, which is only marginally accentuated with age. Finally, we show that transplantation imposes severe constraints on HSC engraftment, consistent with the previously observed oligoclonal HSC activity under these conditions. Thus, we uncover fundamental differences between the normal maintenance of the haematopoietic system, its regulation by challenge, and its re-establishment after transplantation. HSC fate mapping and its linked modelling provide a quantitative framework for studying *in situ* the regulation of haematopoiesis in health and disease.

The paucity of HSCs has largely impeded direct measurements of their functions *in situ*. To determine fundamental properties (frequencies of active HSCs, fluxes between stem and progenitor compartments, residence time and expansion in compartments) of unperturbed steady-state haematopoiesis[13], we devised an experimental system for inducible genetic marking of HSCs *in situ*. As driver for Cre recombinase (Cre) we used the *Tie2* (also known as *Tek*) locus, which is expressed in embryonic and adult HSCs[14,15]. We generated a knock-in mutant expressing from the *Tie2* locus a gene encoding codon-improved Cre (iCre) fused to two modified oestrogen receptor binding domains (designated MCM)[16] (Extended Data Fig. 1a–c). We chose this weakly inducible and tightly regulated system to prevent leakiness. The *Tie2*^{MCM} allele was crossed to *Rosa*^{YFP} mice expressing the yellow fluorescent protein (YFP) reporter in a Cre-dependent manner. In the absence of tamoxifen, we did not detect YFP$^+$ haematopoietic cells in bone marrow, thymus and spleen in *Tie2*$^{MCM/+}$*Rosa*^{YFP} mice ($n = 30$; data not shown). After tamoxifen treatment, MCM becomes active and deletes the stop cassette of the YFP marker gene, thus rendering Cre-expressing cells and their non-Cre-expressing progeny YFP-positive (Extended Data Fig. 1d). Early after treatment (20 days) the labelled cells were almost exclusively HSCs, defined as lineage marker (Lin)$^-$Kit$^+$Sca-1$^+$ (LSK) CD150$^+$CD48$^-$ (refs 3, 17 and 18) (Fig. 1a). In a total of 112 adult *Tie2*$^{MCM/+}$*Rosa*^{YFP} mice, a mean of 1.0% of HSCs were labelled *in situ* after tamoxifen treatment (Extended Data Fig. 1e). Transplantation of a single YFP-marked HSC into genetically conditioned HSC recipients (*Rag2*$^{-/-}$ $\gamma c^{-/-}$ *Kit*$^{W/Wv}$; γc is also known as *Il2rg*)[19] led to long-term donor HSC engraftment and multilineage reconstitution in primary and secondary recipients (Extended Data Fig. 1f), hence initially labelled cells were functional HSCs (Extended Data Table 1). We ruled out the possibility that HSC numbers and functions were compromised by loss of one *Tie2* allele in *Tie2*$^{MCM/+}$ mice in a series of control experiments (Extended Data Fig. 2).

We estimated by limiting dilution analysis frequencies of HSCs contributing to overall haematopoiesis, and to lymphoid and myeloid lineages (Fig. 1b and Extended Data Fig. 1g–j). At least one out of three HSCs contributed YFP$^+$CD45$^+$ progeny in the bone marrow between 6 and 34 weeks after labelling. This is the overall and cumulative frequency regardless of the type of lineage produced, and it represents a lower limit given that all mice with labelled HSCs also contained labelled progeny. Considering 2.8×10^8 total nucleated bone marrow cells per mouse[20], and an HSC frequency of 0.006%, a mouse has ~17,000 HSCs; 30% active HSCs indicates that ~5,000 HSCs contributed to normal haematopoiesis within the observation period. In transplantation experiments,

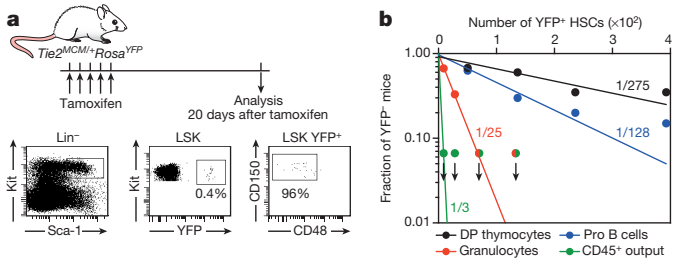

Figure 1 | Inducible HSC labelling in *Tie2*$^{MCM/+}$*Rosa*^{YFP} mice and frequency estimates on HSC output. **a**, Phenotype of labelled cells 20 days after tamoxifen injection. **b**, Limiting dilution analysis of labelled HSCs and lineage output. The fraction of negative mice for YFP-expressing Lin$^+$CD45$^+$ cells (green), granulocytes (red), pro B cells (blue) or double-positive (DP) thymocytes (black) was plotted on a logarithmic scale against the number of YFP$^+$ HSCs (Extended Data Fig. 1g–j). Arrows indicate lower detection limit (no negative mice in these groups).

[1]Division of Cellular Immunology, German Cancer Research Center (DKFZ), Im Neuenheimer Feld 280, D-69120 Heidelberg, Germany. [2]Division of Theoretical Systems Biology, German Cancer Research Center (DKFZ), Im Neuenheimer Feld 280, D-69120 Heidelberg, Germany. [3]Division of Biostatistics, German Cancer Research Center (DKFZ), Im Neuenheimer Feld 280, D-69120 Heidelberg, Germany. [4]Department of Microbiology and Immunology, University of Leuven, B-3000 Leuven, Belgium. [5]Autoimmune Genetics Laboratory, VIB, B-3000 Leuven, Belgium. [6]BIOSS, Centre For Biological Signaling Studies, University of Freiburg, Schänzlestraße 18, D-79104 Freiburg, Germany. [7]Department of Molecular Immunology, BioIII, Faculty of Biology, University of Freiburg, and Max-Planck Institute of Immunobiology and Epigenetics, Stübeweg 51, D-79108 Freiburg, Germany.
*These authors contributed equally to this work.

©2015 Macmillan Publishers Limited. All rights reserved

absolute numbers of contributing HSCs are 100-fold lower[10,11] than our estimate for steady state haematopoiesis. We also determined pathway frequencies from HSCs to granulocytes, and T and B cell progenitors (Fig. 1b and Extended Data Fig. 1g–j). The results revealed correlations between the numbers of labelled HSCs and labelled lineage output, with the (time-averaged) probability for finding labelled granulocytes being five- to tenfold higher than lymphocytes.

To address the fluxes from adult HSCs via stem and progenitor compartments to peripheral lineages, we resolved the output from *in-situ*-labelled HSCs kinetically (Fig. 2a–f). Unexpectedly, up to 3 weeks after induction in adult mice, the label was exclusively retained in HSCs with no label found in LSK $CD150^{-}CD48^{-}$ short-term (ST)-HSCs, and LSK $CD150^{-}CD48^{+}$ multipotent progenitors (MPPs) (Fig. 2b). Within these downstream stem and progenitor compartments, the first marked cells emerged from 4 weeks onwards (Fig. 2c). Beyond 16 weeks, labelled HSCs had contributed to all analysed progenitor and mature cell lineages, with labelled myeloid cells arising sooner than labelled lymphoid cells (Fig. 2e, f). Analysis of overall bone marrow cells further indicated that the label emanates from marked HSCs (Extended Data Fig. 3a). Very few myeloid progenitors (0.010% common myeloid progenitors (CMPs); 0.001% granulocyte–macrophage progenitors (GMPs); 0.006% megakaryocyte–erythroid progenitors (MEPs)) in the bone marrow were also initially marked (Fig. 2b, asterisk), consistent with weak expression of *Tie2* in myeloid progenitors (http://www.immgen.org; data not shown) leading to direct, HSC-independent, labelling. Because of the limited life span of CMPs, GMPs and their progeny (Extended Data Fig. 4), the presence of labelled cells beyond 6 weeks after tamoxifen treatment reflects only cells that have arisen *de novo* from labelled HSCs.

Given the extraordinarily slow label progression out of the adult HSC compartment, we investigated how rapidly HSCs are used during development (Fig. 2g–k and Extended Data Fig. 3b). $Tie2^{MCM/+}Rosa^{YFP}$ mice were treated *in utero* in midgestation (embryonic day (E) 10.5) with tamoxifen. While initially (E12.5) almost exclusively HSCs (but not erythro-myeloid progenitors[21]; Extended Data Fig. 5) were marked in fetal liver, the label progressed within days to progenitors in fetal liver and bone marrow, and by 1 week after birth, equilibrium was nearly reached between labelled HSCs and the entire peripheral system. Hence, HSC use is very rapid (and possibly complete) during development but slow during maintenance of the system (Fig. 2l).

We exploited the kinetic data for adult mice (Fig. 2b–f) to infer the fluxes between stem and progenitor compartments as well as residence time and expansion of the cells in the compartments (Fig. 3). In a given reference compartment (for example, ST-HSCs) the cells lost by onward differentiation (for example, towards MPPs) are replaced by influx from the upstream compartment (for example, HSCs), and by cell production in the reference compartment itself (Fig. 3a). The flux is the product of the rate of differentiation per cell and the total amount of cells undergoing differentiation. The movement of label between compartments contains information on the rate (Fig. 3b), and the ratios of total cell numbers were determined for stem and progenitor compartments (Extended Data Fig. 6a). These considerations form the basis of our model for quantifying the labelling data (Supplementary Methods and Supplementary Discussion).

The steady label frequency of around 1% is consistent with self-renewal of labelled HSCs (Fig. 3c; HSC panel). In compartments downstream from HSCs, labelled cells incrementally replaced non-labelled cells (Fig. 3c). The mathematical model fitted the label frequencies measured up to 240 days after induction, and correctly predicted label frequencies at later time points (Fig. 3c).

We estimated the rates of cell differentiation and net proliferation in the stem and progenitor compartments (Fig. 3d, e, Extended Data Fig. 6b, c and Supplementary Methods). The rate of net proliferation equals the number of cells born per day minus cells lost by death during the same time period. On average, per day, 1 out of 110 HSCs differentiates into an ST-HSC, and 1 out of 22 ST-HSCs differentiates into an MPP (Fig. 3d, f). At the MPP stage, considered a lymphoid–myeloid bifurcation point, we estimate that per day 1 out of 46 MPPs generates a CLP, while 1 MPP generates 4 CMPs (Fig. 3d, f). Given that the cell numbers also increase from HSC to ST-HSC and MPP (Fig. 3f), the efflux of cells exceeded influx in all of these compartments. To maintain compartment size, this flux difference is balanced by net proliferation (efflux minus influx = net proliferation). The rates of net proliferation

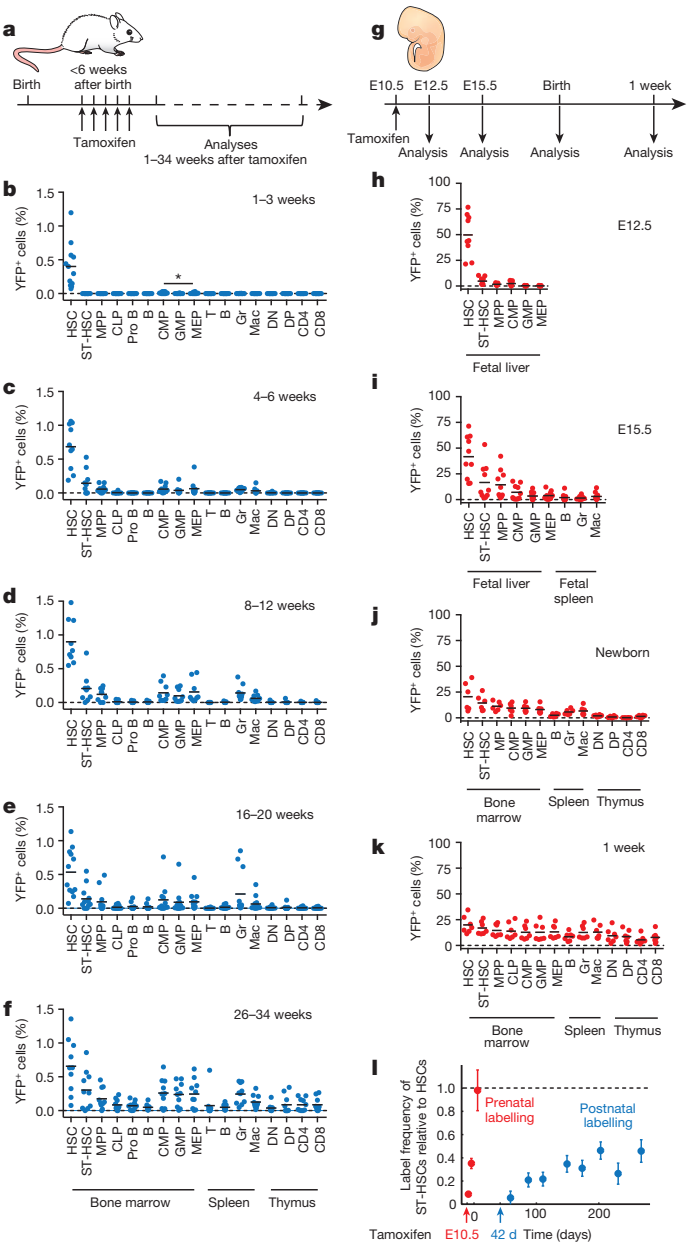

Figure 2 | Label progression through the haematopoietic system during adult maintenance and fetal development. **a**, HSC label induction and output analysis in adult tamoxifen-treated $Tie2^{MCM/+}Rosa^{YFP}$ mice. **b–f**, Percentages of YFP^{+} cells among the indicated haematopoietic cells in bone marrow, spleen and thymus. Mice were analysed at 1–3 (**b**; $n = 12$), 4–6 (**c**; $n = 10$), 8–12 (**d**; $n = 9$), 16–20 (**e**; $n = 12$) and 26–34 (**f**; $n = 10$) weeks after label induction. Dots represent individual mice, and bars indicate the mean. DN, double negative thymocytes; Gr, granulocytes; Mac, macrophages. **g–k**, *In utero* HSC label induction and analysis in fetal, newborn and 1-week-old $Tie2^{MCM/+}Rosa^{YFP}$ mice. YFP labelling frequencies were determined at E12.5 (**h**; $n = 9$), E15.5 (**i**; $n = 10$), in newborns (**j**; $n = 6$) and 1 week after birth (**k**; $n = 8$) for the indicated organs and cells. **l**, Kinetic of label progression from HSCs to ST-HSCs in embryonic (red; $n = 66$) and adult (blue; $n = 110$) mice (n per time points; see Supplementary Methods); arrows indicate tamoxifen treatment. Data are mean and s.e.m.

©2015 Macmillan Publishers Limited. All rights reserved

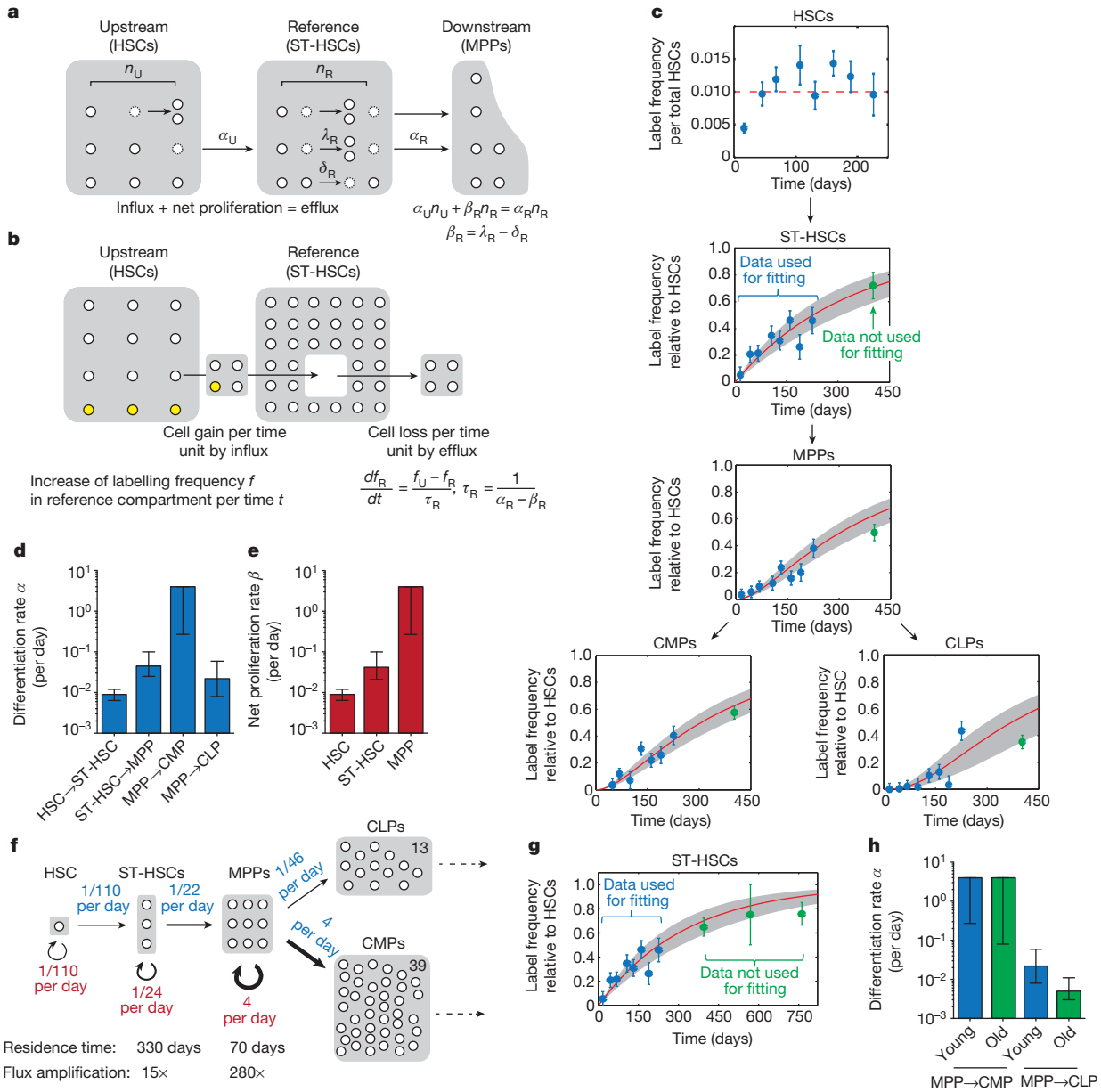

Figure 3 | Inference of stem and progenitor cell differentiation, and proliferation from label progression. **a**, At steady state, the rate of cell loss in a reference compartment due to cell differentiation and death is balanced by cell influx from the upstream compartment, and by proliferation within the reference compartment. This balance relates the total upstream and reference compartment sizes (n_U and n_R, respectively) to the rates of cell differentiation (α_U and α_R) and to net proliferation (proliferation − death) ($\beta_R = \lambda_R - \delta_R$). **b**, The label frequency in the reference compartment (f_R) equilibrates over time with the label frequency in the upstream compartment (f_U). The time for label equilibration $\tau_R = 1/(\alpha_R - \beta_R)$ (residence time) is determined by how rapidly cells are lost from the reference compartment. **c**, HSC label over time (blue dots; red dashed line, average), label progression (blue dots, with s.e.m., as in Fig. 2l), and mathematical model fitting (red lines, best fit; grey shades, 95% confidence bands). Data measured at ~400 days were not used for fitting (green points, $n = 11$ mice) but have been predicted correctly by the model. **d**, **e**, Inferred average rates of cell differentiation (**d**) and net proliferation (**e**) for stem and progenitor cell compartments (with 95% confidence intervals). **f**, Dynamics of stem and progenitor cell compartments inferred from the experimental data. Relative compartment sizes are symbolized by grey boxes, and magnitude of fluxes by arrow width. **g**, The model based on data in young mice (blue dots) also predicts data obtained in very old mice (green dots). **h**, Inferred rates of myeloid and lymphoid differentiation from MPPs in younger (7–238 days after label induction; CMPs only considered beyond 42 days) ($n = 110$) and older (332–802 days) ($n = 41$) mice.

increased from HSC via ST-HSC to MPP compartments, in parallel with the differentiation rates (Fig. 3d, e).

Together, the differentiation rate and net proliferation determine how close a compartment operates to self-renewal. To quantify the degree of self-renewal, we define the residence time in a compartment as the time period in which the compartment would decay to 37% ($1/e$) of its size, if all influx were switched off. The residence time is determined by the duration a cell and its progeny spend in the compartment before being lost by differentiation or cell death. The compartment residence times can be estimated from the labelling data (Supplementary Methods). For HSCs, given that the labelling frequencies are maintained over time (Fig. 3c) despite efflux (Fig. 3d), net proliferation ensures complete self-renewal, and the residence time is theoretically infinite. Linking our estimate of the HSC net proliferation rate (~1 out of 110 per day; Fig. 3e, f) to proliferation measurements would imply that in assays using 5-bromo-2′-deoxyuridine (BrdU) ~1% of HSCs were labelled per day if HSCs lived indefinitely (and ~2% if HSC lifetime was 100 days). This figure is in the order of magnitude of the reported ~4% BrdU labelling per day in the 'HSC-1' population (as a subset of LSK SLAM-defined HSCs)[18], suggesting that the Tie2$^+$ HSCs we label *in situ* reside at the top of

©2015 Macmillan Publishers Limited. All rights reserved

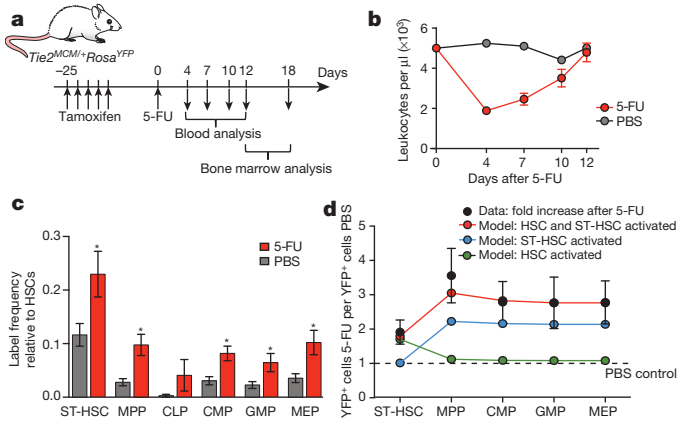

Figure 4 | *In situ* HSC response to 5-FU challenge. **a**, Experimental outline. **b**, Mean of absolute leukocyte numbers in peripheral blood on the indicated days after 5-FU ($n = 12$, red dots) or PBS ($n = 9$, black dots) injections. **c**, Labelling frequencies of the indicated populations relative to HSCs after 5-FU ($n = 18$, red bars) or PBS ($n = 15$, grey bars) (mean from days 12 and 18). *$P = 0.031$ (ST-HSCs), 0.003 (MPPs), 0.213 (CLPs), 0.002 (CMPs), 0.034 (GMPs) and 0.013 (MEPs) (two-tailed *t*-test assuming non-equal variances; 5-FU versus PBS). **d**, Simulated increase (coloured dots and lines) in YFP labelling frequencies considering participation of HSCs and/or ST-HSCs versus experimental data (black dots; ratios of 5-FU over PBS frequencies, taken from **c**). Error bars denote s.e.m.

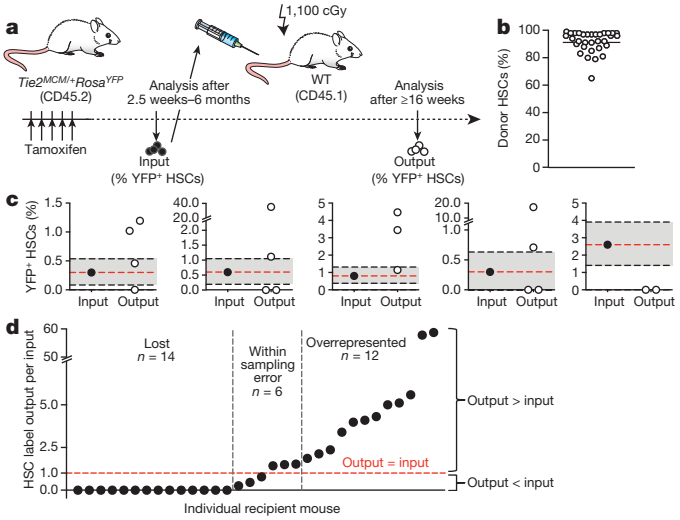

Figure 5 | Fate of *in-situ*-labelled HSCs after bone marrow transplantation. **a**, Experimental outline. **b**, Chimaerism of donor HSCs in recipient mice ($n = 32$) (mean, horizontal line). **c**, Frequencies of YFP$^+$ HSCs (black dots; level indicated by red dashed lines) in individual donor mice, and of YFP$^+$ donor HSCs (white dots) in the corresponding recipient mice. Representative data from a total of 11 donors and 32 recipients are shown. Grey shaded areas denote 95% confidence intervals of sampling errors. **d**, Ratio of engrafted HSC label output over donor HSC input. Red dashed line (ratio = 1) indicates equal output and input ($n = 32$ recipients).

the HSC hierarchy. For ST-HSCs, net proliferation almost accounts for the efflux towards MPPs, and the compartment requires only minimal influx from HSCs. Hence, even ST-HSCs operate near self-renewal, their residence time is exceedingly long (330 days), and label progression does not reach equilibrium within the ~2-year lifetime of a mouse (Fig. 3g). Substantial self-renewal (residence time 70 days) was found even at the MPP stage. Proliferation of MPPs leads to an efflux of cells into common lymphoid progenitors (CLPs) and CMPs that is approximately ~280 times the influx from ST-HSCs (Fig. 3f), making the MPPs a key amplifier. We also analysed progenitor compartments downstream from CLPs (pro B) and CMPs (MEPs and GMPs) (Extended Data Fig. 6d).

An imbalance between myeloid and lymphoid production has been viewed as an age-dependent HSC property[22]. We used fate mapping to re-address this question independent of transplantation, and found a marked myeloid bias that, however, was only marginally accentuated with age through relative loss of lymphoid potential (Fig. 3h). Such bias could be caused by skewed differentiation from a common progenitor, or by preferential proliferation in the myeloid branch. Phenotypes and designations of tested progenitors at putative branch points are shown in Extended Data Fig. 7. In both scenarios, which are not mutually exclusive, production of CMPs was several-hundred-fold larger than that of CLP.

To examine the responsiveness of haematopoiesis to perturbation, we challenged HSC-labelled mice with a single injection of 5-fluoruracil (5-FU), a cytotoxic agent causing a transient leukopenia in the blood (Fig. 4a, b). After peripheral rebound, we observed higher stem and progenitor cell labelling frequencies, relative to HSC labelling, than in untreated mice (Fig. 4c). This accelerated label equilibration between HSCs and subsequent compartments after haematopoietic injury indicates feedback inhibition on HSCs output under steady state. These data are fit by a model in which the kinetics of net proliferation and differentiation are accelerated (at least) in both HSC and ST-HSC compartments, but not in either alone (Fig. 4d and Supplementary Discussion).

Output from highly polyclonal HSCs in adult haematopoiesis *in situ* (Fig. 1b) is in contrast to oligoclonal HSC activity found in transplantation experiments[7–12]. To address this discrepancy, we followed the fate of *in-situ*-marked HSCs after conventional bone marrow transplantation. Adult *Tie2*$^{MCM/+}$*Rosa*^{YFP} mice were treated with tamoxifen, and Lin$^-$Kit$^+$ bone marrow cells from each donor (CD45.2) were transplanted into 1–4 lethally irradiated recipients (CD45.1) (Fig. 5a). For each donor, the HSC labelling frequency was recorded before transplantation ('input'). Despite uniformly strong donor HSC engraftment after 16–18 weeks (average 90%; Fig. 5b), the percentages of YFP-marked cells among total donor HSC ('output') were highly variable compared to the input frequencies in individual recipients (Fig. 5c). Input and output were roughly equal (within sampling error) in only 6 out of 32 recipients, whereas in most recipients donor HSCs were either lost (14 out of 32) or overrepresented (12 out of 32) (Fig. 5d). We estimate that on average 1 out of 33 donor HSCs engrafted (Extended Data Fig. 8a–c). In two extreme cases, YFP$^+$ donor HSCs represented only 0.3% or 0.6% of the input, but 17% or 35%, respectively, of the output, suggesting much stronger proliferation than for HSCs under steady state (Extended Data Fig. 8d and Supplementary Discussion). In summary, the participation of individual engrafted HSCs to the repopulation of the bone marrow is highly heterogeneous.

Inducible labelling of HSCs in normal mouse bone marrow showed that during development HSCs are rapidly used to establish the haematopoietic system. Once this is accomplished, individual HSCs are only rarely active, but over time a large portion of HSCs contributes to adult haematopoiesis. Indeed, although the mean HSC labelling frequency was low, all mice with marked HSCs produced labelled progeny, indicating that a large fraction, or at least 30%, of all HSCs contributes to haematopoiesis in adult mice after label induction. By contrast, previous work based on barcoding showed that few HSCs actively drive haematopoiesis after transplantation. We re-addressed HSC diversity in the wake of transplantation, avoiding potential pitfalls of cellular heterogeneity of mixing experiments. The observed HSC oligoclonality is hence a hallmark of post-transplantation but not normal unperturbed haematopoiesis. These findings indicate that experimental and possibly also clinical HSC transplantations are based on a much smaller stem cell foundation than physiological haematopoiesis.

HSC proliferation has often been taken as a proxy for asymmetric cell division (for example, ref. 23) and, also indirectly, as measure of differentiation rates. Proliferation may, however, not only yield differentiating progeny but also compensate for cell loss, precluding proliferation as an unambiguous marker of differentiation rates. Here, we quantified haematopoietic flux based on label progression from HSCs. Our data

©2015 Macmillan Publishers Limited. All rights reserved

support in principle an order of differentiation *in situ* from HSCs to ST-HSCs and MPPs and onwards. However, in divergence from the idea of a continuous stream from the top of a haematopoietic pyramid, a very low flux emanated from HSCs. While ST-HSCs are relatively short-lived on transplantation, *in situ* this compartment is exceedingly long-lived because ST-HSC self-renewal is almost sufficient to make up for the cell loss by differentiation. We hence identified this compartment as the primary source of haematopoietic maintenance in mice. This reservoir property of ST-HSCs readily explains the apparent HSC-independence of haematopoiesis noted in a recent report[24]. However, to maintain the ST-HSC compartment in the long run (>1 year), it requires continuous input from HSCs; we estimate that per day 150 HSCs feed into this compartment (17,000 total HSC × 1/110 differentiating per day). Hence, true HSC deficiency may go unnoticed for extended periods of time while functionally impaired ST-HSC and MPP compartments would cause rapid signs of acute bone marrow failure (Extended Data Fig. 9).

Collectively, HSCs act in development as founding stem cells, and in adult mice as replenishing cells, ST-HSCs as long-term amplifying cells, and MPPs as intermediate-term amplifying cells. The described fate-mapping system may also visualize responses to haematopoietic challenges imposed by cancer, infections, cachexia or ageing. The accelerated HSC output in response to haematopoietic injury by treatment with 5-FU underscores this outlook.

Online Content Methods, along with any additional Extended Data display items and Source Data, are available in the online version of the paper; references unique to these sections appear only in the online paper.

Received 11 July 2014; accepted 19 January 2015.
Published online 11 February 2015.

1. Smith, L. G., Weissman, I. L. & Heimfeld, S. Clonal analysis of hematopoietic stem-cell differentiation *in vivo*. *Proc. Natl Acad. Sci. USA* **88,** 2788–2792 (1991).
2. Osawa, M., Hanada, K., Hamada, H. & Nakauchi, H. Long-term lymphohematopoietic reconstitution by a single CD34-low/negative hematopoietic stem cell. *Science* **273,** 242–245 (1996).
3. Kiel, M. J., Yilmaz, O. H., Iwashita, T., Terhorst, C. & Morrison, S. J. SLAM family receptors distinguish hematopoietic stem and progenitor cells and reveal endothelial niches for stem cells. *Cell* **121,** 1109–1121 (2005).
4. Sieburg, H. B. *et al.* The hematopoietic stem compartment consists of a limited number of discrete stem cell subsets. *Blood* **107,** 2311–2316 (2006).
5. Dykstra, B. *et al.* Long-term propagation of distinct hematopoietic differentiation programs *in vivo*. *Cell Stem Cell* **1,** 218–229 (2007).
6. Abramson, S., Miller, R. G. & Phillips, R. A. The identification in adult bone marrow of pluripotent and restricted stem cells of the myeloid and lymphoid systems. *J. Exp. Med.* **145,** 1567–1579 (1977).
7. Keller, G., Paige, C., Gilboa, E. & Wagner, E. F. Expression of a foreign gene in myeloid and lymphoid cells derived from multipotent haematopoietic precursors. *Nature* **318,** 149–154 (1985).
8. Lemischka, I. R., Raulet, D. H. & Mulligan, R. C. Developmental potential and dynamic behavior of hematopoietic stem cells. *Cell* **45,** 917–927 (1986).
9. Dick, J. E., Magli, M. C., Huszar, D., Phillips, R. A. & Bernstein, A. Introduction of a selectable gene into primitive stem cells capable of long-term reconstitution of the hemopoietic system of *W/W^v* mice. *Cell* **42,** 71–79 (1985).
10. Gerrits, A. *et al.* Cellular barcoding tool for clonal analysis in the hematopoietic system. *Blood* **115,** 2610–2618 (2010).
11. Lu, R., Neff, N. F., Quake, S. R. & Weissman, I. L. Tracking single hematopoietic stem cells *in vivo* using high-throughput sequencing in conjunction with viral genetic barcoding. *Nature Biotechnol.* **29,** 928–933 (2011).
12. Naik, S. H. *et al.* Diverse and heritable lineage imprinting of early haematopoietic progenitors. *Nature* **496,** 229–232 (2013).
13. Harrison, D. E., Lerner, C., Hoppe, P. C., Carlson, G. A. & Alling, D. Large numbers of primitive stem cells are active simultaneously in aggregated embryo chimeric mice. *Blood* **69,** 773–777 (1987).
14. Yano, M. *et al.* Expression and function of murine receptor tyrosine kinases, TIE and TEK, in hematopoietic stem cells. *Blood* **89,** 4317–4326 (1997).
15. Hsu, H. C. *et al.* Hematopoietic stem cells express Tie-2 receptor in the murine fetal liver. *Blood* **96,** 3757–3762 (2000).
16. Zhang, Y. *et al.* Inducible site-directed recombination in mouse embryonic stem cells. *Nucleic Acids Res.* **24,** 543–548 (1996).
17. Weissman, I. L. Stem cells: units of development, units of regeneration, and units in evolution. *Cell* **100,** 157–168 (2000).
18. Oguro, H., Ding, L. & Morrison, S. J. SLAM family markers resolve functionally distinct subpopulations of hematopoietic stem cells and multipotent progenitors. *Cell Stem Cell* **13,** 102–116 (2013).
19. Waskow, C. *et al.* Hematopoietic stem cell transplantation without irradiation. *Nature Methods* **6,** 267–269 (2009).
20. Boggs, D. R. The total marrow mass of the mouse: a simplified method of measurement. *Am. J. Hematol.* **16,** 277–286 (1984).
21. Gomez Perdiguero, E. *et al.* Tissue-resident macrophages originate from yolk sac-derived erythro-myeloid progenitors. *Nature* http://dx.doi.org/10.1038/nature13989 (2014).
22. Geiger, H., de Haan, G. & Florian, M. C. The ageing haematopoietic stem cell compartment. *Nature Rev. Immunol.* **13,** 376–389 (2013).
23. Wilson, A. *et al.* Hematopoietic stem cells reversibly switch from dormancy to self-renewal during homeostasis and repair. *Cell* **135,** 1118–1129 (2008).
24. Sun, J. *et al.* Clonal dynamics of native haematopoiesis. *Nature* **514,** 322–327 (2014).

Supplementary Information is available in the online version of the paper.

Acknowledgements We thank C. Blum for blastocyst injections, T. Arnsperger, N. Maltry and S. Schäfer for technical assistance, and the animal facility at the DKFZ for expert mouse husbandry. We are grateful to N. Dietlein, H. J. Fehling, T. Feyerabend, C. Opitz, J. Rodewald, A. Roers, K. Rajewsky and A. Trumpp for discussions. K.B. was initially funded through the International Graduate School in Molecular Medicine, Ulm. M.R. was supported by the DFG through EXC294, TRR130 and SFB746. T.H. is a member of CellNetworks, and was supported by BMBF e:Bio grant T-Sys (Fkz 031614) and EU-FP7 Marie Curie ITN Quantitative T cell immunology (QuanTI). H.-R.R. was supported by DFG-SFB 873-project B11, DFG-SFB 938 project L, ERC Advanced Grant no. 233074, and the Helmholtz Alliance on preclinical cancer models (PCCC).

Author Contributions K.B. designed and performed experiments, K.K. and S.M.S. performed experiments, M.B. and M.F. performed theoretical modelling, T.H.-L. made initial bioinformatic analyses, M.R. contributed to the tamoxifen-regulated Cre construct, T.H. developed mathematical models and wrote the paper, and H.-R.R. conceived and supervised the study, and wrote the paper.

Author Information Reprints and permissions information is available at www.nature.com/reprints. The authors declare no competing financial interests. Readers are welcome to comment on the online version of the paper. Correspondence and requests for materials should be addressed to H.-R.R. (hr.rodewald@dkfz.de) or T.H. (t.hoefer@dkfz.de).

©2015 Macmillan Publishers Limited. All rights reserved

METHODS

Generation of *Tie2*$^{MCM/+}$ knock-in mice. For inducible marking of HSC *in situ* we used the *Tie2* locus as driver for Cre recombinase (Cre). Because conventional Cre was insufficient for inducible HSC labelling in our first *Tie2* knock-in mutant, we constructed a second one in which we inserted a gene encoding codon-improved Cre (iCre) fused to two modified oestrogen receptor binding domains, referred to as MCM[16], into the first exon of the *Tie2* locus by homologous recombination in embryonic stem cells. The targeting strategy is depicted schematically in Extended Data Fig. 1a. The targeting construct consisted, from 5′ to 3′, of a short homologous arm (from −1898 to −1 base pairs (bp)) upstream of the ATG start codon of the *Tie2* gene (ENSMUSG00000006386), a splice donor site, an intron and a splice acceptor site (intron), all taken from the rabbit β-hemoglobin (*HBB2*) gene[25], the coding sequence of codon-improved Cre[26] flanked by two mutated oestrogen receptor sites[16,27], a poly-adenylation signal (pA) from the rabbit β-hemoglobin gene, a FRT-flanked neomycin (*Neo*) resistance gene, a long homologous arm (nucleotides +4 to +4983 of the *Tie2* gene, considering the adenine in the ATG start codon as position +1), and finally the diphtheria toxin subunit A gene (*DT-A*) for selection against random integration. This weakly inducible and tightly regulated system was chosen to prevent leakiness[28]. The complete nucleotide sequence of the final targeting vector can be obtained from the authors on request. Gene targeting experiments were performed in E14.1 embryonic stem cells. Correct homologous recombination of the targeting vector resulted in replacement of the start codon (nucleotides +1 to +3) in the first exon of the *Tie2* locus with the MCM cassette. Correctly targeted clones were first identified by PCR. Targeted embryonic stem cell clones were transiently transfected with a plasmid (pCAGGS-FlpE-GFP) expressing Flp-recombinase (gift from H. J. Fehling) to delete the *Neo* cassette. Site-specific integration and *Neo* deletion were confirmed by Southern blotting. DNA was digested with BspHI. Blots were hybridized with a radiolabelled 1.0-kb iCre-specific probe. All *Tie2* gene sequences upstream and downstream of exon 1 are preserved in the *Tie2*^{MCM} allele. A *Neo*-deficient embryonic stem cell subclone (*Tie2*$^{MCM\Delta Neo}$) was injected into C57BL/6 blastocysts, and chimaeric mice were backcrossed to C57BL/6 mice to transmit the *Tie2*^{MCM} allele. Heterozygous *Tie2*$^{MCM/+}$ mice are fertile and show no apparent abnormalities. Homozygous *Tie2*$^{MCM/MCM}$ embryos die between E9.5 and E12.5, as previously described for *Tie2*$^{-/-}$ mice[29,30].

Induction of reporter gene expression by tamoxifen. *Tie2*$^{MCM/+}$ mice were crossed to *Rosa*^{YFP} (Gt(ROSA)26Sor$^{tm1.1(EYFP)Cos}$) mice[31]. Tamoxifen (1 g; Sigma T5648) was dissolved in 4 ml ethanol absolute and 36 ml peanut oil (Sigma P2144) at 55 °C. Aliquots of tamoxifen (25 mg ml^{-1}) were stored at −20 °C and heated to 37 °C shortly before usage. Mice were injected daily on 5 consecutive days with 1 mg tamoxifen intraperitoneally. For *in utero* tamoxifen treatments the day of the plug was regarded as day 0.5 of the pregnancy (E0.5). Pregnant mice were treated by oral gavage on E7.5 or E10.5 with a single dose of 2.5 mg tamoxifen and 1.75 mg progesterone (Sigma P0130) to counteract late fetal abortions. Delivery of the pups was routinely assisted by caesarean section at E20.5, and mice were raised by foster mothers.

Flow cytometry. Bone marrow cells were flushed from femurs, tibias, coxa and humeri using PBS supplemented with 5% heat-inactivated FCS in PBS. Cells were filtered through a 20-μm filter (Falcon). Spleens, thymi and fetal organs were directly mashed in a 20-μm filter with a plunger of a syringe. Fc receptors were blocked by incubating cells in 5% FCS with purified mouse IgG (500 μg ml^{-1}, Jackson ImmunoResearch Laboratories). All stainings were performed in 5% FCS on ice for 30 min with optimal dilutions of commercially-prepared antibodies. Reagents used were CD3ε allophycocyanin (APC) (17A2), CD3ε eFluor780 (17A2), CD3ε phycoerythrin (PE) (145-C11), CD4 PE-Cy7 (GK1.5), CD8 APC (53-6.7), CD11b PE (M1/70), CD11b PE-Cy7 (M1/70), CD11b PerCP Cy5.5 (M1/70), CD16/32 PE-Cy7 (93), CD16/32 PE-Cy5.5 (93), CD19 PerCP-Cy5.5 (ID3), CD34 eFluor660 (RAM34), CD45 PE-Cy7 (30-F11), CD45.1 eFluor660 (A20), CD45.2 PE (104), CD48 APC (HM 48-1), CD48 PE (HM 48-1), CD117 eFluor780 (2B8), CD127 PE-Cy7 (A7R34), CD135 PE (A2F10), Sca-1 PE-Cy7 (D7), Sca-1 PerCP-Cy5.5 (D7), Tie2 biotin (bio) (TEK4), Tie2 PE (TEK4) (eBioscience), CD3ε bio (500A2), CD4 bio (GK1.5), CD4 PE (H129.19), CD8 bio (53-6.7), CD8 PE (53-6.7), CD11b APC (M1/70), CD19 APC (1D3), CD19 bio (1D3), CD19 PE (1D3), CD45 bio (30-F11), Gr-1 APC (RB6-8C5), Gr-1 bio (RB6-8C5), Gr-1 PE (RB6-8C5), IgM bio (R6-60.2), IgM PE (R6-60.2), Streptavidin PE-Cy7, Sca-1 PE (E13 161.7), Ter119 APC (Ter119), Ter119 bio (Ter119), Ter119 PE (Ter119) (BD Pharmingen), CD4 APC (RM4.5), CD19 QDot605 (6D9), streptavidin APC, streptavidin QDot605, Sca-1 PE-Cy5.5 (D7) (Invitrogen/Molecular Probes), CD11b bio (M1/70.15) (Caltag), CD135 bio (A2F19), CD150 PE-Cy7 (TC15-12F12.2), CD229 PE (Ly9AB3) (Biolegend). The lineage cocktail (Lin) was composed of CD3ε, CD4, CD8, CD11b, CD19, Gr-1 and Ter119. To enrich for Lin-negative progenitor populations, bone marrow cells were stained with lineage markers followed by depletion with Dynabeads (Life technologies) according to the manufacturer's instruction. Dead cells were excluded by staining with Sytox Blue (Invitrogen). Cells were analysed on a FACSFortessa, or sorted by FACSAriaIII (all Becton & Dickinson), and data were analysed by BD FACSDiva software. Bone marrow cell populations were defined as follows: HSCs (Lin$^-$Kit$^+$Sca-1$^+$CD150$^+$CD48$^-$), ST-HSCs (Lin$^-$Kit$^+$Sca-1$^+$CD150$^-$CD48$^-$), ST-HSCs CD229$^-$, ST-HSCs CD229$^+$, MPPs (Lin$^-$Kit$^+$Sca-1$^+$CD150$^-$CD48$^+$), CLPs (Lin$^-$IL7R$^+$Flk2$^+$Kit^{low}Sca-1^{low}), pro B cells (CD19$^+$IgM$^-$), B cells (CD19$^+$IgM$^+$), CMPs (Lin$^-$Kit$^+$Sca-1$^-$CD34$^+$CD16/32^{low}), GMPs (Lin$^-$Kit$^+$Sca-1$^-$CD34$^+$CD16/32$^+$) and MEPs (Lin$^-$Kit$^+$Sca-1$^-$CD34$^-$CD16/32$^-$). Populations in the spleen were defined as follows: T cells (CD3$^+$CD19$^-$CD11b$^-$Gr-1$^-$), B cells (CD19$^+$CD3$^-$CD11b$^-$Gr-1$^-$), granulocytes (Gr-1$^+$CD11b$^+$CD3$^-$CD19$^-$) and macrophages (CD11b$^+$Gr-1$^-$CD3$^-$CD19$^-$). The populations in the thymus were defined as follows: double-negative thymocytes (CD4$^-$CD8$^-$) (DN), double-positive thymocytes (CD4$^+$CD8$^+$) (DP), CD4$^+$ thymocytes (CD4$^+$CD8$^-$) (CD4) or CD8$^+$ thymocytes (CD4$^-$CD8$^+$) (CD8). Erythromyeloid progenitors (Lin$^-$Kit$^+$CD45$^{+/low}$) in fetal liver were defined as described previously[21,32].

Mice. Mice carrying constitutively active reporter alleles (*panYFP* or *panRFP*) were generated by crossing *Rosa*^{YFP} or *Rosa*^{dtRFP} reporter mice[31,33] to germline Cre-deleter mice[34]. Offspring constitutively expressing YFP or RFP in all tissues were backcrossed towards the C57BL/6 background, and used in competitive transplantation experiments (Extended Data Fig. 2h, i) and in adoptive transfers of myeloid and lymphoid progenitors (Extended Data Fig. 4). *Rag2*$^{-/-}$ *γc*$^{-/-}$ *Kit*$^{W/Wv}$ mice[19] were used for adoptive transfer experiments without previous irradiation (Extended Data Figs 1f, 2h, i and 4). For transfer experiments with irradiation, congenic B6.SJL-Ptprca Pep3b/BoyJ (H-2^b; CD45.1$^+$) mice were used as recipients (Fig. 5). All animal procedures were approved by the Regierungspräsidium Karlsruhe, and performed in accordance with the Institutional Guidelines. Both male and female mice were used at ages ranging from embryonic E12.5 to around 120 weeks (2 years). No mice were excluded from the analysis. No randomization and no blinding were used.

PCR genotyping. Tissues were lysed in lysis buffer (DirectPCR-Lysis Reagent Tail, Peqlab) according to the manufacturer's instruction. Mice were genotyped by PCR for 2 min at 94 °C (20 s at 94 °C, 30 s at 51 °C, 1 min at 72 °C) 35 times; 10 min at 72 °C using a common 5′ oligonucleotide annealing upstream of the rabbit β-hemaglobin gene (5′-CATCGCATACCATACATAGGTGGAGG-3′) and a 3′ oligonucleotide annealing to the rabbit β-hemaglobin gene (5′-AATCAAGGGTCC CCAAACTCAC-3′), yielding a 526-bp DNA fragment indicating the *Tie2*^{MCM} allele, and a 3′ oligonucleotide (5′-GAGGCAGCATCTGTCTACAAGAGATGG-3′), yielding a 745-bp DNA fragment indicating the *Tie2*$^+$ allele.

Single-cell transplantation. YFP$^+$ HSCs (LSK CD150$^+$CD48$^-$) were isolated from tamoxifen-treated *Tie2*$^{MCM/+}$*Rosa*^{YFP} mice by electronic single-cell deposition into individual wells of a U-bottom 96-well plate containing 100 μl sterile 5% FCS. Before injection, 100 μl sterile PBS was added to each well, and single cells were injected intravenously into individual *Rag2*$^{-/-}$ *γc*$^{-/-}$ *Kit*$^{W/Wv}$ recipients. Peripheral blood samples were collected 4–8 weeks after transfer from the submandibular vein into EDTA-containing microtubes (Sarstedt) to screen for progeny of donor cells (detected by YFP expression). Organs of recipient mice were analysed at least 16 weeks after transplantation as shown in Extended Data Fig. 1f. For secondary transplantations, YFP$^+$Lin$^-$Kit$^+$ bone marrow cells from the primary recipients were purified by cell sorting and 3×10^4 cells were intraveneously injected into individual *Rag2*$^{-/-}$ *γc*$^{-/-}$ *Kit*$^{W/Wv}$ recipients. At least 16 weeks after transfer organs were analysed by flow cytometry.

Competitive transplantation. Equal cell numbers (500–1,000 of each) of HSCs (LSK CD150$^+$CD48$^-$) from *Tie2*$^{MCM/+}$ mice (either with *panRFP* reporter allele or without), and wild-type competitor HSCs (LSK CD150$^+$CD48$^-$) from *Tie2*$^{+/+}$ mice (*panYFP*) were co-injected intraveneously into *Rag2*$^{-/-}$ *γc*$^{-/-}$ *Kit*$^{W/Wv}$ recipient mice. Peripheral blood samples were collected 4–8 weeks after transfer to screen for progeny of donor cells (not shown), and after at least 16 weeks the organs indicated in Extended Data Fig. 2 were analysed for the contributions of progeny from *Tie2*$^{MCM/+}$ or *Tie2*$^{+/+}$ HSC. To assess the life span of myeloid progenitor and mature granulocytes, cell-sorter-purified CMPs and GMPs (mixed as one population) from *panRFP* mice were intraveneously injected together with CLPs from *panYFP* mice into *Rag2*$^{-/-}$ *γc*$^{-/-}$ *Kit*$^{W/Wv}$ recipient mice (5×10^4 CMPs plus GMPs and 0.5×10^4 CLPs per mouse). Peripheral blood samples were collected 7, 14, 21 and 32 days after transplantation from the submandibular vein into EDTA-containing microtubes (Sarstedt) to screen by flow cytometry for donor-derived progeny cells.

Transplantation into lethally irradiated mice. Lin-negative Kit$^+$ cells from tamoxifen-treated *Tie2*$^{MCM/+}$*Rosa*^{YFP} mice (CD45.2) were sorted and 0.5×10^5–2.0×10^5 cells injected intraveneously into lethally irradiated (1,100 cGy; split dose with 4 h time gap between each dose; Cesium 137 GammaCell40 Irradiator, Besttheratronics) congenic B6.SJL-Ptprca Pep3b/BoyJ mice. Recipient mice were maintained on antibiotic water (1.17 g l^{-1} neomycin sulphate) for 14 days. Bone marrow of recipient mice was analysed after at least 16 weeks after transplantation.

Proliferation assay. *Tie2*$^{MCM/+}$ and *Tie2*$^{+/+}$ littermate mice were injected intraperitoneally with 1 mg EdU (Invitrogen) in PBS. After 24 h, the bone marrow was

©2015 Macmillan Publishers Limited. All rights reserved

collected, cells were stained with the appropriate antibodies before sorting cell-surface receptor Tie2-positive (LSK $Tie2^{+}CD150^{+}CD48^{-}$) and cell-surface receptor Tie2-negative (LSK $Tie2^{-}CD150^{+}CD48^{-}$) HSCs, each from $Tie2^{MCM/+}$ and $Tie2^{+/+}$ littermates. Cells were collected in individual tubes containing 50% FCS, fixed and permeabilized, and the Click-it reaction was performed using the Click-iT EdU Flow Cytometry Assay Kit (Invitrogen) according to the manufacturer's protocol.

5-FU treatment. 5-FU (Sigma F6627) was dissolved in sterile PBS, and tamoxifen-treated $Tie2^{MCM/+}Rosa^{YFP}$ mice were intravenously injected with a single dose of 250 mg kg^{-1} or PBS. Mice were maintained on antibiotic (1.17 g neomycin sulphate per litre of drinking water) for 14 days. Peripheral blood was collected 4, 7, 10 and 12 days after 5-FU from the submandibular vein into EDTA-containing microtubes (Sarstedt). Absolute numbers of leukocytes per microlitre blood were determined by flow cytometry using anti CD45 PE-Cy7 (30-F11; eBioscience) antibody and APC-conjugated CaliBRITE Beads (BD Biosciences) as standard. On day 12 or 18 after 5-FU treatment bone marrow cells were isolated and analysed by flow cytometry. With two-tailed *t*-test, effect size $d = 1$, $\alpha = 0.05$ and power 0.8, group sizes should be 17 per sample group. We chose $n = 15$ (control) and $n = 18$ (5-FU treatment).

Mathematical methods. Mathematical modelling and parameter inference from the experimental data are described in the Supplementary Information. The corresponding Matlab codes are available on request. No statistical methods were used to predetermine sample size, except for 5-FU treatment.

25. Kouskoff, V., Fehling, H. J., Lemeur, M., Benoist, C. & Mathis, D. A vector driving the expression of foreign cDNAs in the MHC class II-positive cells of transgenic mice. *J. Immunol. Methods* **166,** 287–291 (1993).
26. Shimshek, D. R. *et al.* Codon-improved Cre recombinase (iCre) expression in the mouse. *Genesis* **32,** 19–26 (2002).
27. Verrou, C., Zhang, Y., Zurn, C., Schamel, W. W. & Reth, M. Comparison of the tamoxifen regulated chimeric Cre recombinases MerCreMer and CreMer. *Biol. Chem.* **380,** 1435–1438 (1999).
28. Casanova, E. *et al.* ER-based double iCre fusion protein allows partial recombination in forebrain. *Genesis* **34,** 208–214 (2002).
29. Dumont, D. J. *et al.* Dominant-negative and targeted null mutations in the endothelial receptor tyrosine kinase, *tek*, reveal a critical role in vasculogenesis of the embryo. *Genes Dev.* **8,** 1897–1909 (1994).
30. Sato, T. N. *et al.* Distinct roles of the receptor tyrosine kinases Tie-1 and Tie-2 in blood vessel formation. *Nature* **376,** 70–74 (1995).
31. Srinivas, S. *et al.* Cre reporter strains produced by targeted insertion of EYFP and ECFP into the ROSA26 locus. *BMC Dev. Biol.* **1,** 4 (2001).
32. Bertrand, J. Y. *et al.* Three pathways to mature macrophages in the early mouse yolk sac. *Blood* **106,** 3004–3011 (2005).
33. Luche, H., Weber, O., Nageswara Rao, T., Blum, C. & Fehling, H. J. Faithful activation of an extra-bright red fluorescent protein in ''knock-in'' Cre-reporter mice ideally suited for lineage tracing studies. *Eur. J. Immunol.* **37,** 43–53 (2007).
34. Schwenk, F., Baron, U. & Rajewsky, K. A *cre*-transgenic mouse strain for the ubiquitous deletion of *loxP*-flanked gene segments including deletion in germ cells. *Nucleic Acids Res.* **23,** 5080–5081 (1995).

©2015 **Macmillan Publishers Limited. All rights reserved**

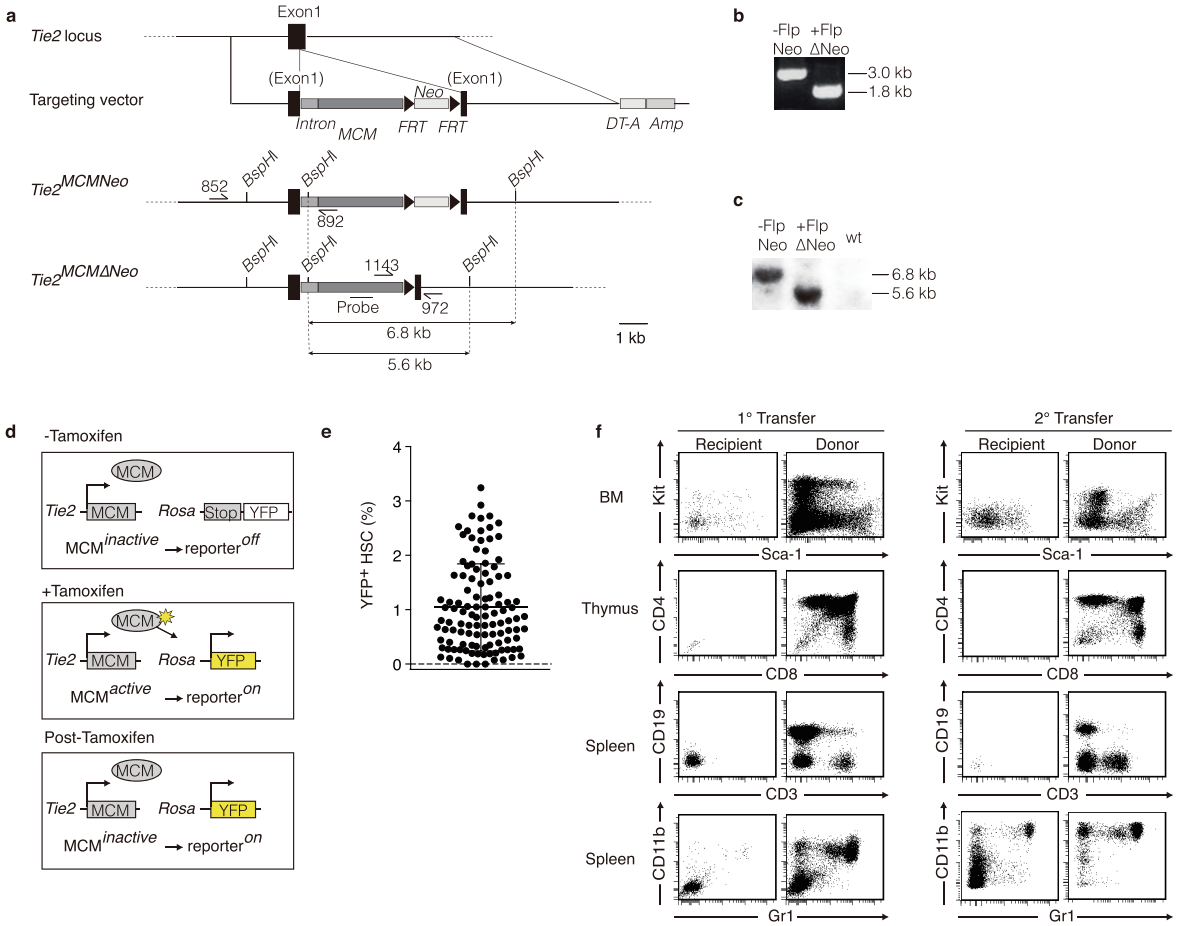

Group	Nr of mice	Mean YFP$^+$ HSC (%)	Total number of YFP$^+$ HSC per mouse*	Fraction of YFP$^-$ mice for CD45$^+$	Fraction of YFP$^-$ mice for Gr
I	15	0.0515	9	0/15†	10/15
II	15	0.1682	28	0/15†	5/15
III	15	0.4175	70	0/15†	1/15
IV	15	0.7938	133	0/15†	1/15

* Total number of HSC per mouse ~16,800 (ref. 20)
† For graphical illustration fraction was counted as 1/15

Group	Nr of mice	Mean YFP$^+$ HSC (%)	Total number of YFP$^+$ HSC per mouse*	Fraction of YFP$^-$ mice for pro B	Fraction of YFP$^-$ mice for DP
I	19	0.2993	50	12/19	13/19
II	20	0.8112	136	6/20	12/20
III	20	1.4036	236	4/20	7/20
IV	20	2.3378	393	3/20	7/20

* Total number of HSC per mouse ~16,800 (ref. 20)

Extended Data Figure 1 | Generation of the *Tie2^{MCM}* allele, labelling of HSCs in tamoxifen-treated *Tie2$^{MCM/+}$Rosa^{YFP}* mice, and groups for limiting dilution analysis. **a**, The endogenous *Tie2* locus, the gene targeting vector and the targeted allele with (*Tie2^{MCMNeo}*) and without (*Tie2^{MCMΔNeo}*) neomycin are depicted. Oligonucleotides and DNA probe for genotyping, and restriction sites used for Southern blotting are indicated (not drawn to scale). **b**, PCR verification of the targeted *Tie2^{MCM}* allele in embryonic stem cells before and after neomycin deletion. **c**, Southern blot analysis of *Tie2^{MCMNeo}* (−Flp) and *Tie2^{MCMΔNeo}* (+Flp), and wild-type embryonic stem-cell clones. **d**, Principle of inducible fate mapping. In the absence of tamoxifen MCM is inactive (reporter^{off}). Tamoxifen treatment activates the reporter (reporter^{on}). After tamoxifen treatment, labelled cells and their progeny remain marked (reporter^{on}). **e**, Summary of HSC labelling frequencies of tamoxifen-treated *Tie2$^{MCM/+}$Rosa^{YFP}* mice ($n = 112$; 5 times on 5 consecutive days) analysed between 1 and 34 weeks after label induction. These data are the basis for the kinetic analysis (Fig. 2a–f) and for the mathematical modelling (Fig. 3). Each dot represents an individual mouse. Bar indicates mean (1.041 ± 0.8013 s.d.). **f**, A single YFP$^+$ LSK CD150$^+$CD48$^-$ HSC from a tamoxifen-treated *Tie2$^{MCM/+}$Rosa^{YFP}* mouse was transplanted into a *Rag2$^{-/-}$ γc$^{-/-}$ Kit$^{W/Wv}$* recipient mouse (1° transfer). Donor cells were identified by YFP expression, and analysed 16 weeks after transplantation in bone marrow (BM), thymus and spleen using the markers shown. YFP$^+$Kit$^+$ donor bone marrow cells were re-transplanted into a secondary *Rag2$^{-/-}$ γc$^{-/-}$ Kit$^{W/Wv}$* recipient (2° transfer), and analysed as described for the primary transfer. **g**–**j**, HSC labelling frequencies in tamoxifen-treated *Tie2$^{MCM/+}$Rosa^{YFP}* mice analysed 6 weeks onwards after label induction were used for limiting dilution analysis of CD45$^+$ output, granulocytes ($n = 60$) (**g**, **h**), pro B cells and double-positive thymocytes ($n = 79$) (**i**, **j**). Each dot represents an individual mouse. Mice grouped together are highlighted in black or white (groups I–IV). Mathematical calculations are shown in the tables (**h**, **j**). In **g**, data shown represent the aggregate of labelling frequencies below 1% shown in **e**, plus data obtained in mice receiving only a single tamoxifen injection.

©2015 Macmillan Publishers Limited. All rights reserved

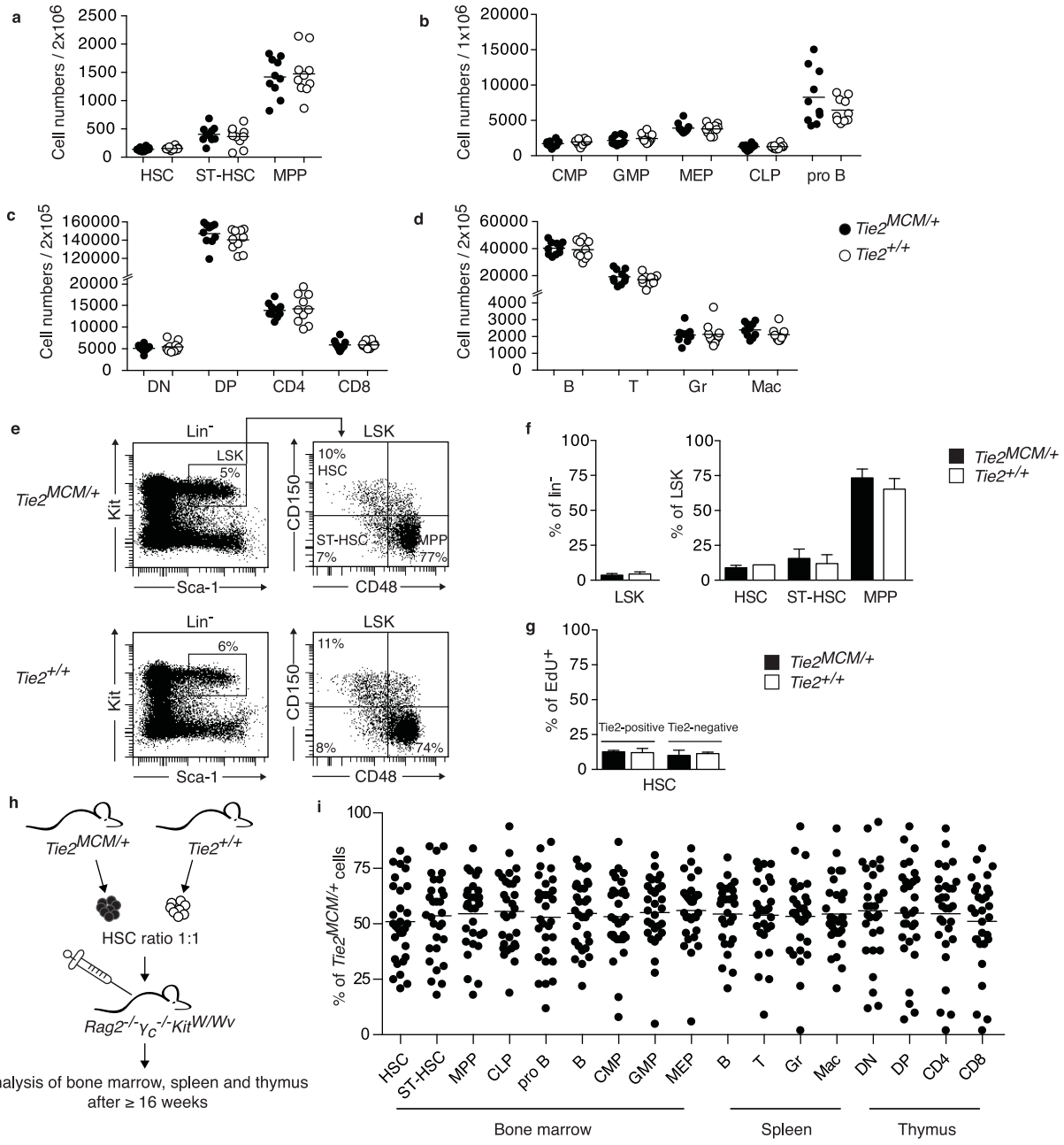

Extended Data Figure 2 | Characterization of *Tie2*$^{MCM/+}$ mice. **a**–**d**, Numbers of haematopoietic cell subsets isolated from bone marrow (**a**, **b**), thymus (**c**) and spleen (**d**) of *Tie2*$^{MCM/+}$ ($n = 10$; black) and *Tie2*$^{+/+}$ ($n = 10$; white) littermates were determined by flow cytometry. Each dot represents an individual mouse. Bars indicate mean. **e**, **f**, Flow cytometric analysis of a representative *Tie2*$^{MCM/+}$ (top) and *Tie2*$^{+/+}$ (bottom) mouse gated on Lin$^-$ cells, and analysed for expression of Kit versus Sca-1. Further analysis of Lin$^-$Kit$^+$Sca-1$^+$ (LSK) cells for CD150 and CD48 revealed comparable marker distributions (**f**). Percentages of LSK cells among the Lin$^-$ fraction (left), and of HSCs, ST-HSCs and MPPs among the LSK fraction (right) in the bone marrow of three independent *Tie2*$^{MCM/+}$ (black) and *Tie2*$^{+/+}$ (white) mice. Data are mean ± s.d. **g**, Proliferation rates in surface receptor Tie2-positive and Tie2-negative HSCs in the bone marrow of *Tie2*$^{MCM/+}$ (black) and *Tie2*$^{+/+}$ (white) mice 24 h after EdU administration. Data represent mean ± s.d. from two independent experiments of FACS-sorted populations from *Tie2*$^{MCM/+}$ ($n_{Exp1} = 5$; $n_{Exp2} = 3$) and *Tie2*$^{+/+}$ ($n_{Exp1} = 3$; $n_{Exp2} = 2$) mice. **h**, **i**, *Rag2*$^{-/-}\gamma c^{-/-}$ *Kit*$^{W/Wv}$ recipients ($n = 30$; for analysis of B and T cells in the spleen $n = 28$) were injected with equivalent numbers of *Tie2*$^{MCM/+}$ and *Tie2*$^{+/+}$ HSCs (500–1,000 of each), and analysed after at least 16 weeks. The percentages of *Tie2*$^{MCM/+}$ HSC-derived haematopoietic cells in bone marrow, spleen and thymus are shown. Each dot represents an individual mouse. Bars indicate mean.

©2015 Macmillan Publishers Limited. All rights reserved

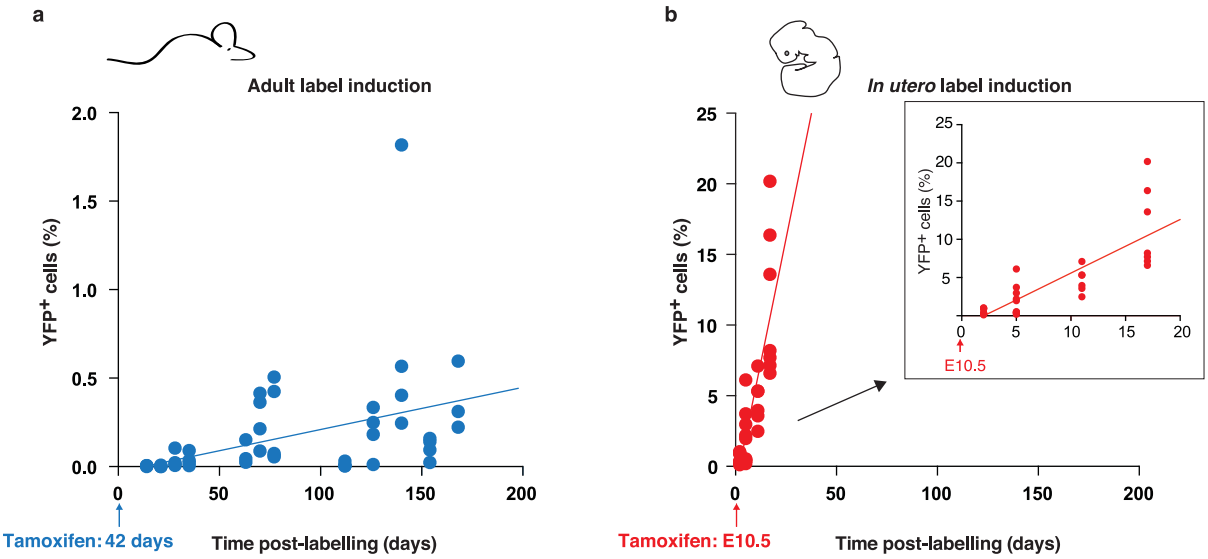

Extended Data Figure 3 | Kinetics of YFP label emergence after label induction in total bone marrow cells in adult mice, and in fetal liver and bone marrow cells in fetal and early postnatal mice. **a**, Percentages of YFP^+ cells among total non-lineage-depleted bone marrow cells of tamoxifen-treated $Tie2^{MCM/+}Rosa^{YFP}$ mice ($n = 47$). Time point 0 corresponds to the time of tamoxifen treatment of adult mice (all of which were at least 6 weeks). **b**, $Tie2^{MCM/+}Rosa^{YFP}$ mice ($n = 32$) were treated with tamoxifen on E10.5 (time point 0). Subsequently, percentages of YFP^+ cells were determined among total fetal liver on E12.5 and E15.5, and in bone marrow at birth and 1 week of age. Each dot represents an individual mouse.

©2015 Macmillan Publishers Limited. All rights reserved

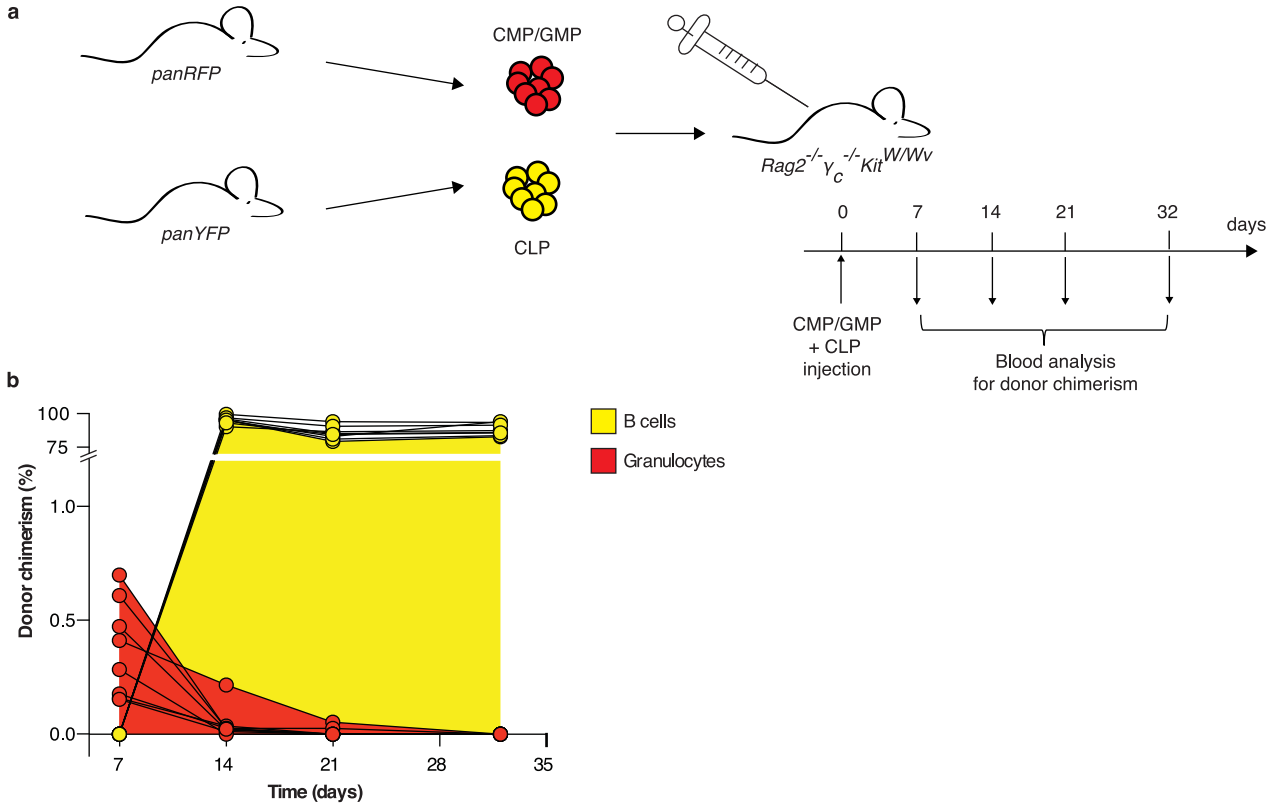

Extended Data Figure 4 | Donor-derived myeloid cells disappear within 6 weeks after adoptive transfer. **a**, *Rag2*$^{-/-}$ $\gamma c^{-/-}$ *Kit*$^{W/Wv}$ recipient mice ($n = 8$) received CMPs and GMPs (together 5×10^4 per mouse) from *panRFP* mice together with CLPs (0.5×10^4 per mouse) from *panYFP* mice. Peripheral blood samples were measured 7, 14, 21 and 32 days after transplantation. **b**, Analysis of donor chimaerism of CMP/GMP-derived (Gr-1$^+$CD11b$^+$ granulocytes, red) and CLP-derived (CD19$^+$ B cells, yellow) progeny. Each line represents an individual mouse.

©2015 Macmillan Publishers Limited. All rights reserved

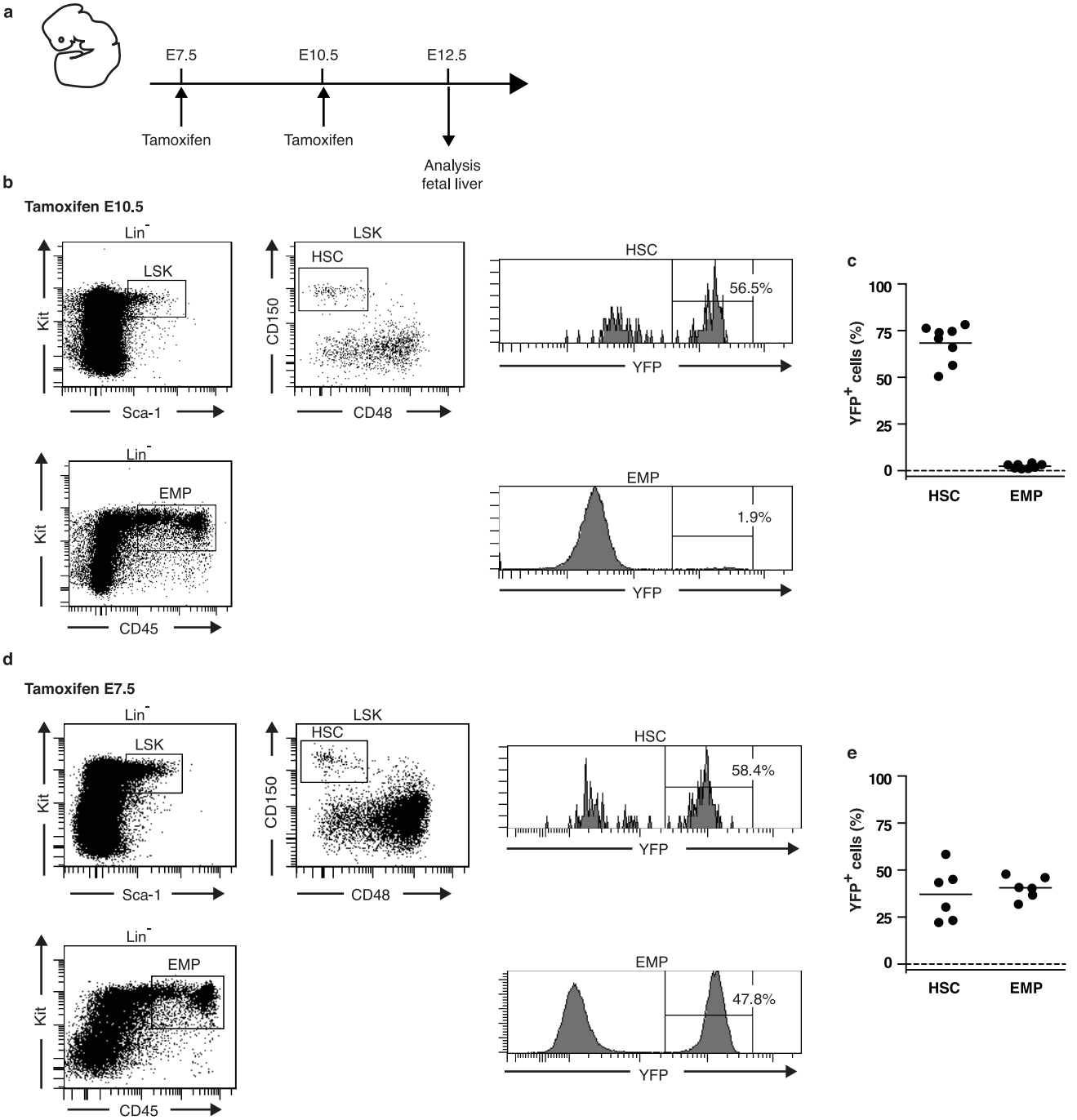

Extended Data Figure 5 | Labelling of HSCs, but not erythromyeloid progenitors, in *Tie2*$^{MCM/+}$*Rosa*^{YFP} embryos treated on E10.5 *in utero* by tamoxifen. **a**, *Tie2*$^{MCM/+}$*Rosa*^{YFP} embryos were treated with tamoxifen on E7.5 or E10.5, and analysed at E12.5. **b**–**e**, Fetal liver cells from representative *Tie2*$^{MCM/+}$*Rosa*^{YFP} embryos labelled on E10.5 (**b**) or E7.5 (**d**) were analysed by flow cytometry for YFP labelling in HSCs (LSK CD150^{+}CD48^{-}) and erythromyeloid progenitors (EMP) (Lin^{-}Kit^{+}CD45$^{+/low}$) (see Methods for references). HSCs were marked in mice labelled at E7.5 and E10.5, but erythromyeloid progenitors were not marked in mice labelled on E10.5. **c**, **d**, Summary of experiments depicted in **b** ($n = 8$) (**c**) and **d** ($n = 6$) (**e**). Each dot represents an individual embryo. Bars indicate mean.

©2015 Macmillan Publishers Limited. All rights reserved

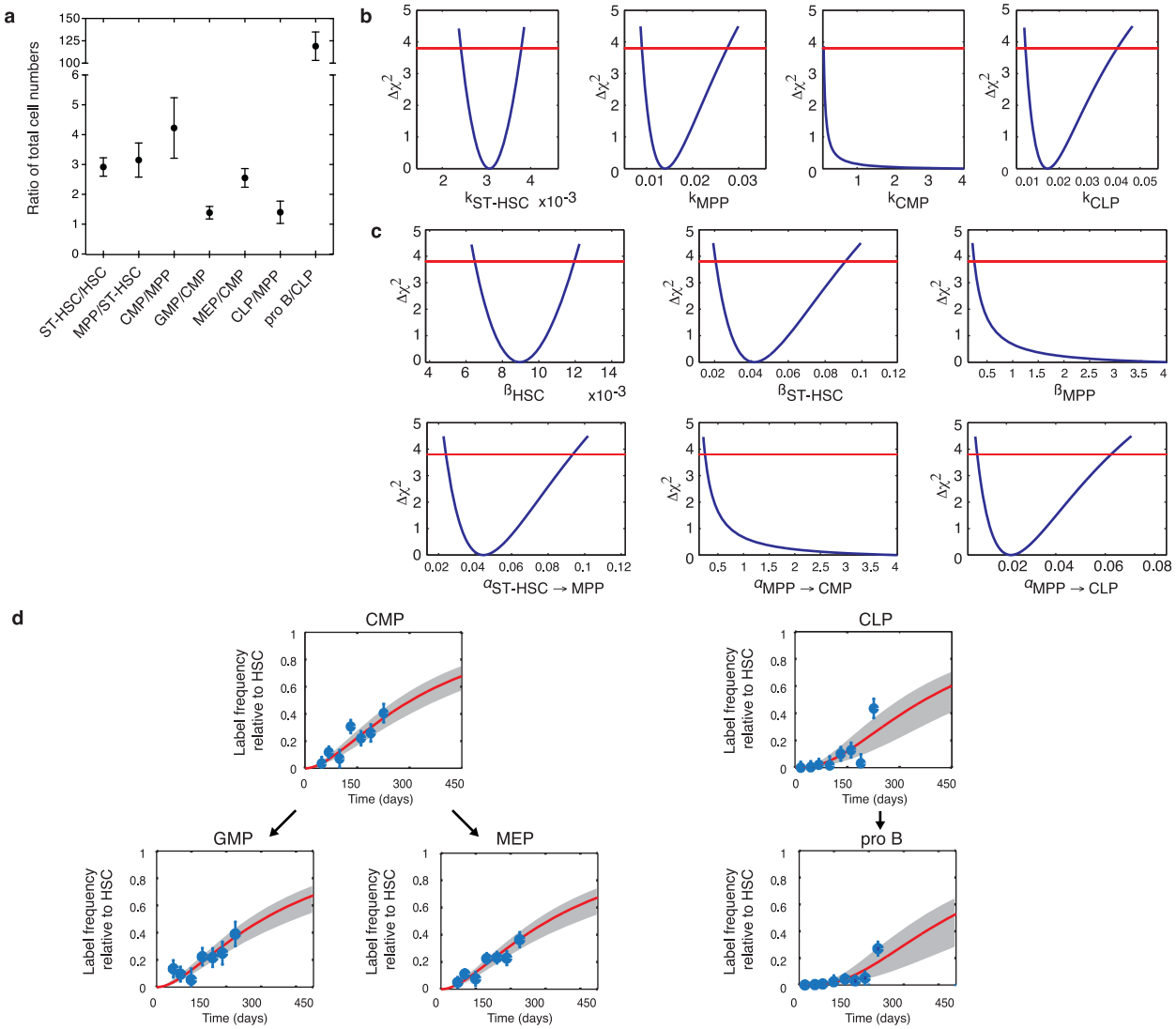

Extended Data Figure 6 | Details of model analysis. a, Ratio of compartment sizes for stem and progenitor cell compartments. Compartment sizes were determined by cell counting of cell suspensions from bone marrow, spleen and thymus in a Neubauer chamber combined with phenotypic definition of each population by flow cytometry. Mean and s.e.m. for $n = 10$ mice are shown. **b**, Confidence bounds for the model parameters. Profile likelihoods (blue lines) for the inverse residence times, $k = 1/\tau$, of cells in the ST-HSC, MPP, CMP and CLP compartments (units: per day). The profile likelihoods have been computed as described in Supplementary Methods, with the experimental data from Fig. 3c. The red lines indicate the 95% confidence level. Except for the CMPs, for which the data are consistent with a broad range of k (that is, the CMP residence time is low), the residence times are accurately determined by the label propagation data alone. In particular, the very low k for the ST-HSCs shows that this compartment operates near self-renewal. **c**, Profile likelihoods (blue lines) and 95% confidence level (red lines) for the net proliferation rates (β) and differentiation rates (α), computed with the data of Fig. 3c and Extended Data Fig. 4 (unit: per day). The differentiation rate from HSCs ($\alpha_{\mathrm{HSC}\to\mathrm{ST\text{-}HSC}}$) has the same profile likelihood as the net proliferation of HSC (β_{HSC}) and is therefore not shown. $\alpha_{\mathrm{HSC}\to\mathrm{ST\text{-}HSC}}$, $\alpha_{\mathrm{ST\text{-}HSC}\to\mathrm{MPP}}$, $\alpha_{\mathrm{MPP}\to\mathrm{CLP}}$, β_{HSC} and $\beta_{\mathrm{ST\text{-}HSC}}$ are accurately determined by the data. Moreover, both $\alpha_{\mathrm{MPP}\to\mathrm{CMP}}$ and β_{MPP} have a lower bound that is one and two orders of magnitude larger than the respective parameters for ST-HSCs and HSCs, showing that MPPs have significantly higher proliferation and differentiation activities than the preceding compartments. Note that (β_{MPP}) and $\alpha_{\mathrm{MPP}\to\mathrm{CMP}}$ are strongly correlated (not shown). **d**, Label progression data and fit of the mathematical model for further downstream myeloid precursors (CMPs to GMPs or MEPs) and lymphoid precursors (CLPs to pro B cells) in the bone marrow. Data were measured up to 238 days after label induction (blue points, with s.e.m., as in Fig. 2l) have been used for the model fit (red lines, best fit and grey shades, 95% confidence bands). The parameter values are as in Supplementary Table 1 and, in addition, $\alpha_{\mathrm{CMP}\to\mathrm{GMP}} = 2\ (0.04, 4)\ \mathrm{day}^{-1}$, $\alpha_{\mathrm{CMP}\to\mathrm{MEP}} = 3\ (0.1, 4)\ \mathrm{day}^{-1}$, $\alpha_{\mathrm{CLP}\to\mathrm{pro\ B}} = 2\ (0.8, 4)\ \mathrm{day}^{-1}$, $\beta_{\mathrm{CMP}} = 4\ (-1, 4)\ \mathrm{day}^{-1}$, $\beta_{\mathrm{CLP}} = 3\ (0.4, 4)\ \mathrm{day}^{-1}$, $\tau_{\mathrm{GMP}} = 0.12\ (0.12, 33)$ days, $\tau_{\mathrm{MEP}} = 0.13\ (0.13, 22)$ days, $\tau_{\mathrm{proB}} = 54\ (6, 141)$ days (in brackets: 95% confidence bounds). For further details see Supplementary Information.

©2015 Macmillan Publishers Limited. All rights reserved

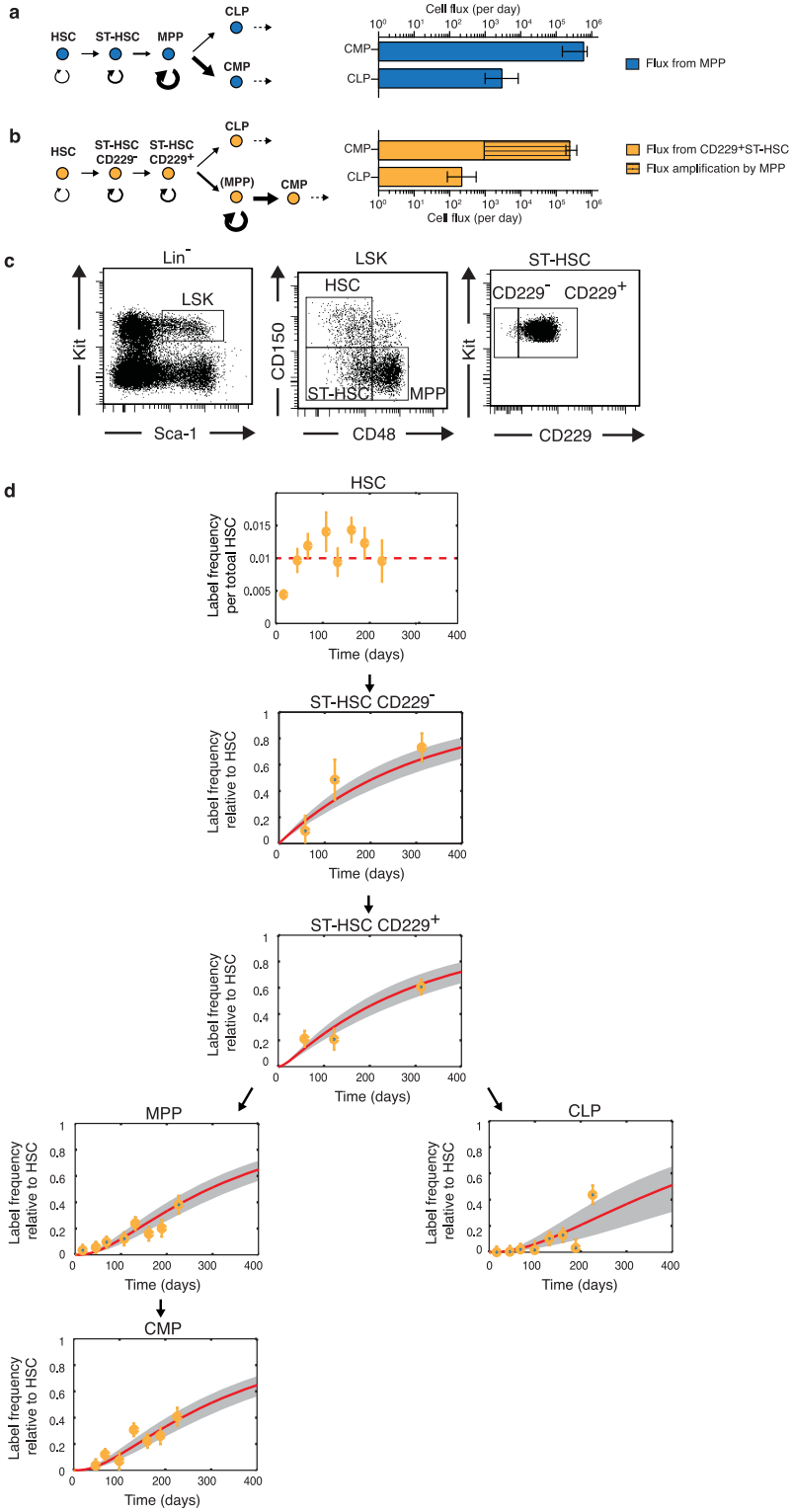

Extended Data Figure 7 | Consequences of lymphoid–myeloid branch points at distinct stem or progenitor stages. **a**–**c**, Lymphoid–myeloid branch points were considered at the MPP stage (**a**) or at the earlier CD229$^+$ ST-HSC subset (**b**). Each population is phenotypically defined as shown in **c**. MPPs have also been termed HPC-1, and the CD229$^+$ ST-HSC subset has also been termed MPP2/3 (ref. 18). Cell flux rates per day are shown from the branch points to CMPs or CLPs (right panels in **a** and **b**, with 95% confidence intervals). In both scenarios, the production of CMPs is several-hundred-fold larger than that of CLPs. Assuming the branch point at the CD229$^+$ ST-HSC stage, biased myeloid differentiation is still evident (~5-fold), but the large uneven production is mainly achieved by flux amplification downstream from the bifurcation. **d**, Label progression data and fit of the mathematical model. Data measured up to 311 days after label induction in the ST-HSC CD229$^-$ and ST-HSC CD229$^+$ compartments (orange points, with s.e.m.; groups of mice: 57 days $n = 7$; 122 days $n = 4$; 311 days $n = 8$) and in CLP, MPP and CMP compartments data measured up to 238 days (orange points, with s.e.m.; groups of adult mice as in Fig. 2l) have been used for the model fit (red lines, best fit; grey shades, 95% confidence bands). The resulting parameters are $\alpha_{HSC \rightarrow CD229\text{–}ST\text{-}HSC} = 0.0001$ (0.00001–0.00016) day^{-1}, $\alpha_{CD229\text{–}ST\text{-}HSC \rightarrow CD229+ST\text{-}HSC} = 4$ (2–4) day^{-1}, $\alpha_{CD229+ST\text{-}HSC \rightarrow MPP} = 0.03$ (0.02–0.06) day^{-1}, $\alpha_{CD229+ST\text{-}HSC \rightarrow CLP} = 0.007$ (0.004–0.012) day^{-1}, $\beta_{CD229\text{–}ST\text{-}HSC} = 4$ (2–4) day^{-1}, $\beta_{CD229+ST\text{-}HSC} = 0.0$ (−0.06–0.0016) day^{-1} and $\beta_{MPP} = 4$ (0.3–4) day^{-1} (in brackets: 95% confidence intervals). For further details see Supplementary Methods.

©2015 Macmillan Publishers Limited. All rights reserved

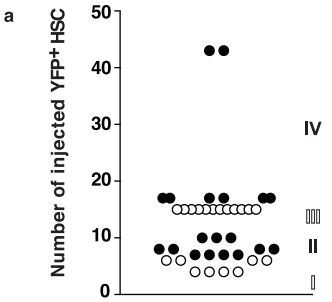

b

Group	Nr of recipients	Mean of injected YFP+ donor HSC per recipient	Fraction of YFP- recipients for HSC
I	8	5	5/8
II	11	8	6/11
III	12	15	6/12
IV	8	24	5/8

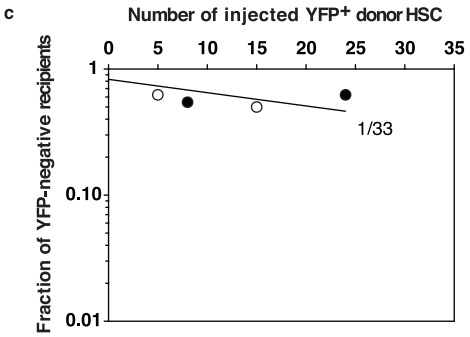

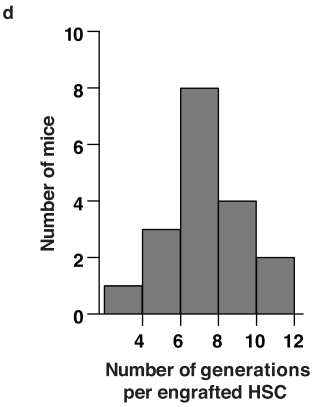

Extended Data Figure 8 | Limiting dilution analysis of *in-situ*-labelled transplanted HSCs. **a**, *Tie2*$^{MCM/+}$*Rosa*^{YFP} mice were injected with tamoxifen (donor bone marrow; see Fig. 5a). Numbers of YFP$^+$ HSCs in donor bone marrow transplanted into 38 recipient mice are displayed. Each dot is an individual recipient. Mice grouped together are highlighted in black or white (groups I–IV). **b**, Data underlying limiting dilution analysis. **c**, Numbers of injected YFP$^+$ donor HSCs are plotted against the fraction of YFP-negative recipients on a logarithmic scale. **d**, Histogram showing the extent of self-renewing proliferation for engrafted YFP$^+$ HSCs in mice labelled 'within sampling error' and 'overrepresented' in Fig. 5d ($n = 18$). Proliferation is shown as the number of generations per engrafted HSC needed to achieve the measured frequencies of YFP$^+$ HSCs in the bone marrow 4 months after transplantation. For further details see Supplementary Discussion.

©2015 Macmillan Publishers Limited. All rights reserved

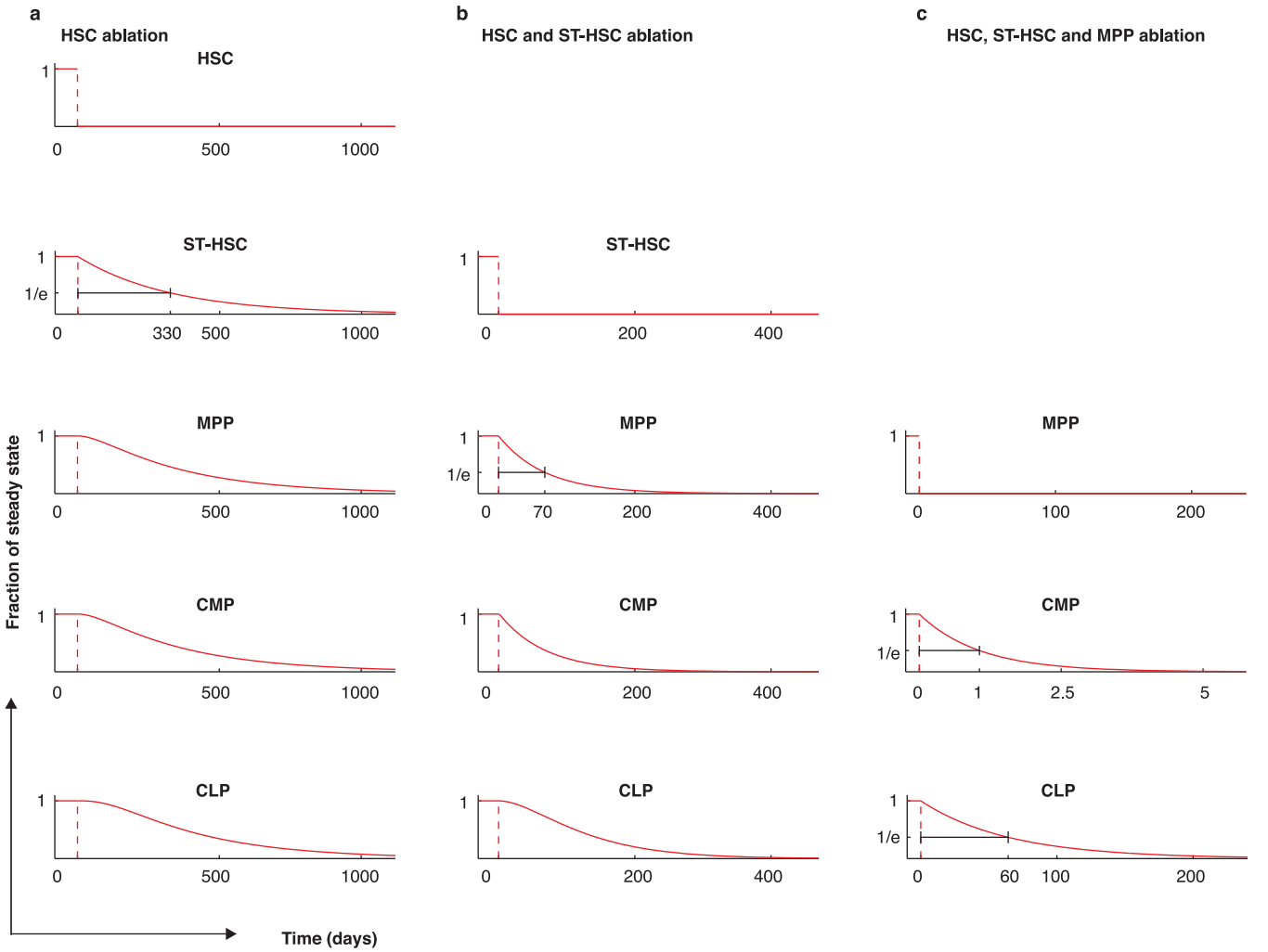

Extended Data Figure 9 | Simulated effects of ablation of HSCs, ST-HSCs or MPPs. In the mathematical model used to fit the label progression data (Fig. 3c), numbers of HSCs (**a**), HSCs and ST-HSCs (**b**), and HSCs, ST-HSCs and MPPs (**c**) were reduced from its steady state value to zero at $t = 0$, and subsequently held there. The predicted responses in the downstream compartments are shown. The horizontal black lines at $1/e = 37\%$ indicate the residence times of the compartments that control the time scale of the response. Note that these simulations assume that there are no homeostatic mechanisms present within the compartments that could maintain their size independent of input from upstream compartments.

©2015 Macmillan Publishers Limited. All rights reserved

Extended Data Table 1 | Transplantations of *in-situ*-labelled HSC

Fraction	Number of injected donor cells	Number of 1° recipients	1° recipients		Number of 2° recipients	2° recipients	
			Long-term	Transient		Long-term	Transient
LSK CD150$^+$ CD48$^-$ YFP$^+$	1	23	1(4%)	4(17%)	3	1(33%)	2(66%)
LSK CD150$^+$ CD48$^-$ YFP$^+$	5	1	1(100%)	-	n.d.		
LSK CD150$^+$ CD48$^-$ YFP$^+$	8	1	1(100%)	-	n.d.		
LSK YFP$^+$	10	3	1(33%)	2(66%)	3	1(33%)	2(66%)
LSK YFP$^+$	15	3	1(33%)	2(66%)	3	1(33%)	2(66%)
LSK YFP$^+$	18	4	1(33%)	-	3	1(33%)	2(66%)
LSK YFP$^+$	20	3	1(33%)	2(66%)	5	2(40%)	3(60%)
LSK YFP$^+$	40	3	3(100%)	-	9	2(22%)	7(88%)

n.d.: not done

YFP-marked stem cells from tamoxifen-treated *Tie2*$^{MCM/+}$*Rosa*^{YFP} mice were injected into primary and secondary *Rag2*$^{-/-}$ γc$^{-/-}$ *Kit*$^{W/Wv}$ recipient mice. Phenotypes and cell numbers of injected cells, numbers of primary (1°) and secondary (2°) recipients, and reconstitution results are given. Percentages in brackets reflect the proportions of reconstituted mice.

©2015 Macmillan Publishers Limited. All rights reserved